

Observation of a dipole-bound excited state in 4-ethynylphenoxide and comparison with the quadrupole-bound excited state in the isoelectronic 4-cyanophenoxide

Cite as: J. Chem. Phys. **155**, 124305 (2021); <https://doi.org/10.1063/5.0065510>

Submitted: 02 August 2021 • Accepted: 06 September 2021 • Published Online: 23 September 2021

 Yue-Rou Zhang, Dao-Fu Yuan,  Chen-Hui Qian, et al.



View Online



Export Citation



CrossMark

ARTICLES YOU MAY BE INTERESTED IN

[Action spectroscopy of the isolated red Kaede fluorescent protein chromophore](#)

The Journal of Chemical Physics **155**, 124304 (2021); <https://doi.org/10.1063/5.0063258>

[Photodetachment spectroscopy and resonant photoelectron imaging of cryogenically cooled 1-pyrenolate](#)

The Journal of Chemical Physics **154**, 094308 (2021); <https://doi.org/10.1063/5.0043932>

[Self-assembling of the neutral intermediate with chemically bound argon in photoexcited van der Waals complex Ar-I₂](#)

The Journal of Chemical Physics **155**, 124308 (2021); <https://doi.org/10.1063/5.0059414>



Chemical Physics Reviews

First Articles Now Online!

READ NOW >>>



Observation of a dipole-bound excited state in 4-ethynylphenoxide and comparison with the quadrupole-bound excited state in the isoelectronic 4-cyanophenoxide

Cite as: J. Chem. Phys. 155, 124305 (2021); doi: 10.1063/5.0065510

Submitted: 2 August 2021 • Accepted: 6 September 2021 •

Published Online: 23 September 2021



View Online



Export Citation



CrossMark

Yue-Rou Zhang,  Dao-Fu Yuan,^{a)} Chen-Hui Qian,  and Lai-Sheng Wang^{a)} 

AFFILIATIONS

Department of Chemistry, Brown University, Providence, Rhode Island 02912, USA

^{a)} Authors to whom correspondence should be addressed: daofu_yuan@brown.edu and Lai-Sheng_Wang@brown.edu

ABSTRACT

Negative ions do not possess Rydberg states but can have Rydberg-like nonvalence excited states near the electron detachment threshold, including dipole-bound states (DBSs) and quadrupole-bound states (QBSs). While DBSs have been studied extensively, quadrupole-bound excited states have been more rarely observed. 4-cyanophenoxide ($4CP^-$) was the first anion observed to possess a quadrupole-bound excited state 20 cm^{-1} below its detachment threshold. Here, we report the observation of a DBS in the isoelectronic 4-ethynylphenoxide anion ($4EP^-$), providing a rare opportunity to compare the behaviors of a dipole-bound and a quadrupole-bound excited state in a pair of very similar anions. Photodetachment spectroscopy (PDS) of cryogenically cooled $4EP^-$ reveals a DBS 76 cm^{-1} below its detachment threshold. Photoelectron spectroscopy (PES) at 266 nm shows that the electronic structure of $4EP^-$ and $4CP^-$ is nearly identical. The observed vibrational features in both the PDS and PES, as well as autodetachment from the nonvalence excited states, are also found to be similar for both anions. However, resonant two-photon detachment (R2PD) from the bound vibrational ground state is observed to be very different for the DBS in $4EP^-$ and the QBS in $4CP^-$. The R2PD spectra reveal that decays take place from both the DBS and QBS to the respective anion ground electronic states within the 5 ns detachment laser pulse due to internal conversion followed by intramolecular vibrational redistribution and relaxation, but the decay mechanisms appear to be very different. In the R2PD spectrum of $4EP^-$, we observe strong threshold electron signals, which are due to detachment, by the second photon, of highly rotationally excited anions resulted from the decay of the DBS. On the other hand, in the R2PD spectrum of $4CP^-$, we observe well-resolved vibrational peaks due to the three lowest-frequency vibrational modes of $4CP^-$, which are populated from the decay of the QBS. The different behaviors of the R2PD spectra suggest unexpected differences between the relaxation mechanisms of the dipole-bound and quadrupole-bound excited states.

Published under an exclusive license by AIP Publishing. <https://doi.org/10.1063/5.0065510>

I. INTRODUCTION

Even though negative ions do not possess Rydberg states, a stable valence-bound anion can have highly diffuse Rydberg-like excited states near its electron detachment threshold as a result of long-range interactions between the extra electron and the neutral core. Experimental and theoretical studies have shown that diverse mechanisms can contribute to the electron binding in such nonvalence anionic states.^{1–4} Although electron correlation effects are known to play important roles in the electron binding of nonvalence states,^{5,6} the anionic state is called a dipole-bound state

(DBS) when the charge–dipole interaction is dominant.^{1–4} Similarly, quadrupole-bound states (QBSs) can exist for anions, which have neutral cores with vanishing dipole moments but large quadrupole moments.^{6–10} Furthermore, an electron can also be bound due to correlation or polarization effects, leading to the correlation-bound state (CBS)^{11–13} or polarization-bound state (PBS)^{14,15} when the neutral cores possess neither a large dipole nor a quadrupole moment. Since first suggested by Fermi and Teller in 1947,¹⁶ DBS has attracted persistent attention because of its fundamental importance in physics and chemistry.^{1–4,17–34} DBSs play significant roles in electron scattering of polar molecules, DNA damage processes by

low-energy electrons, and anion formation in the interstellar medium under astronomical environments.^{35–38} DBSs have also been considered as the doorway to the formation of valence-bound anions.^{39–41} The transition from a DBS to a valence-bound state (VBS) was first considered for CH_3NO_2^- .³⁹ The dynamics from DBS to VBS was first investigated for iodide–water cluster anions $[\text{I}^-(\text{H}_2\text{O})_n]$ using time-resolved photoelectron spectroscopy (TRPES).⁴² TRPES has also been used to probe the dynamics from a nonvalence excited state to VBS in the $[\text{I}^-(\text{C}_6\text{F}_6)]$ complex.⁴³

However, quadrupole-bound anions have been more rarely observed. Even though Mg_2O_2^- was considered to be the first quadrupole-bound anion experimentally characterized, its relatively large electron binding energy suggested that there should be significant valence character in the electron binding, in addition to strong electron correlation effects.⁴⁴ More convincing evidence of a quadrupole-bound anion was reported for the trans-succinonitrile anion produced using Rydberg electron transfer (RET).⁸ Recently, the binding energy of the trans-succinonitrile anion was measured directly using photoelectron spectroscopy (PES),⁹ as well as the quadrupole-bound 1,4-dicyanocyclohexane anion produced by RET.⁴⁵ The search for quadrupole-bound anions is intrinsically challenging because there is no clear correlation between the magnitude of the quadrupole moment and the electron binding energy for QBS.⁶ The first quadrupole-bound excited state was observed in 4-cyanophenoxide (4CP^-) using photodetachment spectroscopy (PDS) of cryogenically cooled anions.⁴⁶ The neutral 4CP radical has a small dipole moment (0.3 D), but a large quadrupole moment ($Q_{xx} = 5.4$, $Q_{yy} = 15.1$, and $Q_{zz} = -20.5$ D Å), resulting in a binding energy of 20 cm^{-1} for the excited QBS. Very recently, an excited QBS was observed in the tetracyanobenzene anion.¹⁰ The neutral tetracyanobenzene molecule has a large quadrupole moment of $Q_{xx} = 19.3$, $Q_{yy} = -29.5$, and $Q_{zz} = 10.2$ D Å, but no dipole moment, and can form a stable valence-bound anion with an electron affinity of 2.4695 eV. The excited QBS in the tetracyanobenzene anion was found to have a surprisingly large binding energy of 0.2206 eV, suggesting the importance of electron correlation effects.

We have developed an experimental apparatus,⁴⁷ coupling electrospray ionization (ESI), cryogenic ion cooling in a 3D Paul trap, and high-resolution photoelectron imaging. We have shown that this third generation electrospray ionization PES (ESI-PES) apparatus is particularly powerful to investigate nonvalence excited states of valence-bound anions.^{29,48–51} The cold anions afforded by cryogenic cooling allow high-resolution PDS to be obtained, which is essential to search for the ground state of nonvalence excited states, the electron detachment threshold, and most importantly above-threshold vibrational resonances (also known as vibrational Feshbach resonances). We have shown that resonant photoelectron spectroscopy (rPES) can be performed by tuning the detachment laser to the Feshbach resonances, yielding much richer spectroscopic information than conventional PES due to vibrational autodetachment.^{52–54} We found that the vibrational autodetachment was mode-selective with a $\Delta v = -1$ propensity rule.^{29,55,56} It has been demonstrated that the combination of PDS and rPES can allow conformation-selective and tautomer-selective spectroscopy to be performed.^{57–59} Recently, we have observed the first π -type DBS,^{60,61} as well as configuration mixing induced by the electric field of the dipole-bound electron.⁶² The dynamics of vibrational autodetachment from DBS

has been directly probed recently using an ultrafast pump–probe technique.⁶³

The vibrational autodetachment from the excited QBS of 4CP^- was found to be similar to that from DBS with the same mode-selectivity and propensity rule.⁴⁶ A recent pump–probe experiment demonstrates that the autodetachment lifetimes from the vibrational Feshbach resonances in the QBS of 4CP^- are also similar to those in DBS.⁶⁴ The bound vibrational levels of the nonvalence excited states are stable and should be long-lived, allowing resonant two-photon detachment (R2PD) to be observed even with our nano-second detachment lasers. However, we have observed the direct spectroscopic evidence of transitions from the bound vibrational levels of the DBS to valence-bound excited states in R2PD of deprotonated 4,4'-biphenol anion.⁶⁵ In R2PD experiments for both DBS and QBS, we have always observed decays from the bound vibrational levels of the nonvalence excited states to the anion ground states (S_0) within the 5 ns detachment laser pulse, manifested as low kinetic energy electrons (or high binding energy features) produced by the second photon. Even though the ultrafast dynamics of the excited DBS in I^- -complexes have been directly probed by TRPES,^{66,67} the long-time photophysics from the bound nonvalence vibrational states has not been directly probed. A very recent pump–probe experiment has revealed an ultrafast conversion from the bound ground vibrational level of the DBS of 4-iodophenoxide to a repulsive valence state along the C–I bond, leading to dissociation to I^- and $\text{C}_6\text{H}_5\text{O}$ at the asymptotic limit.⁶⁸

In the current article, we present a PES, PDS, rPES, and R2PD study of cryogenically cooled 4-ethynylphenoxide (4EP^-). The 4EP radical is polar with a large dipole moment of 3.8 D, suggesting that 4EP^- should possess a DBS as an electronically excited state near its detachment threshold. More interestingly, 4EP^- and 4CP^- have similar structures and they are isoelectronic, providing a rare opportunity to compare the behaviors of a DBS and a QBS in a pair of nearly identical anions (see the insets of Fig. 1). The electron affinity (EA) of the 4EP radical is measured accurately to be $20\,643\text{ cm}^{-1}$ (2.5594 eV). PDS indeed reveals a DBS for 4EP^- 76 cm^{-1} below its detachment threshold, as well as six vibrational Feshbach resonances. Conventional PES at 266 nm shows that both 4EP^- and 4CP^- have a nearly identical valence electronic structure. The vibrational structures revealed in the PES, PDS, and rPES are also very similar for the two anions. However, the R2PD spectra from the bound ground vibrational levels of the nonvalence excited states are found to be surprisingly different, suggesting different decay mechanisms from the DBS and QBS to the respective anionic ground states. Specifically, strong threshold electrons are observed in the R2PD spectrum of 4EP^- , coming from detachment of highly rotationally excited states in S_0 by the second photon, whereas well-resolved vibrational peaks are observed in the R2PD spectrum of 4CP^- corresponding to the three lowest-frequency vibrational modes of S_0 , populated from the decay of the QBS. Possible mechanisms for the different relaxation behaviors from the bound DBS and QBS levels are discussed.

II. EXPERIMENTAL METHODS

The experiment was conducted using our third generation electrospray ionization PES (ESI-PES) apparatus,⁴⁷ which consists of an ESI source,⁶⁹ a cryogenically cooled 3D Paul trap,⁷⁰ and a

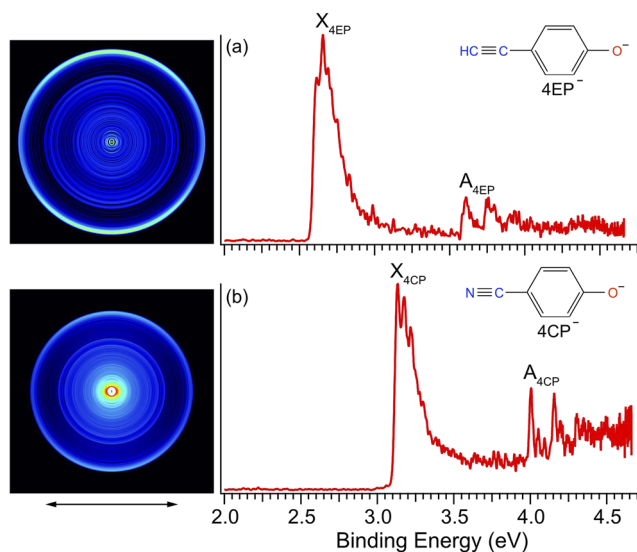


FIG. 1. Photoelectron images and spectra of (a) $4EP^-$ and (b) $4CP^-$ at 266 nm (4.661 eV). The structures of $4EP^-$ and $4CP^-$ are shown in the insets. The double arrow below the images represents the laser polarization.

high-resolution velocity-map imaging (VMI) system.⁷¹ The $4EP^-$ anions were produced by electrospray of a 1 mM solution of 4-ethynylanisole in a CH_3OH/H_2O mixed solvent (9/1 volume ratio) prepared by adding a small amount of NaOH for demethylation. The $4EP^-$ anions from the ESI source were guided into the ion trap by a series of quadrupole and octupole ion guides. The ion trap was cooled to 4.6 K by a two-stage closed cycle helium refrigerator. The anions were collisionally cooled by a mixed He/ H_2 (4/1 volume ratio) buffer gas for 0.1 s before being pulsed into the extraction zone of a time-of-flight mass spectrometer at a 10 Hz repetition rate. The $4EP^-$ anions were mass-selected and photodetached in the interaction zone of the VMI lens by a tunable dye laser. Photoelectrons were focused by the VMI lens onto a pair of 75-mm diameter micro-channel plates coupled to a phosphor screen and captured by a charge-coupled device camera. In addition, we measured the photoelectron images of $4EP^-$ using the fourth (266 nm, 4.661 eV) and the third (355 nm, 3.496 eV) harmonics of a Nd:YAG laser. Similar data were also obtained for $4CP^-$ at 266 nm for comparison. To construct photoelectron spectra from the obtained images, we performed inverse-Abel transformation using both the BASEX and pBASEX programs.^{72,73} The photoelectron spectra were calibrated with the known spectra of Au^- at different photon energies. The kinetic energy (KE) resolution was 3.8 cm^{-1} for 55 cm^{-1} electrons and about 1.5% ($\Delta KE/KE$) for 1 eV electrons in the current experiment.⁴⁷

We also computed the harmonic frequencies of $4EP$ and its dipole moment at the B3LYP/6-311++G^{*,*} level of theory using Gaussian 09, as show in Table S1.⁷⁴

III. RESULTS

A. Comparison of the photoelectron spectra and electronic structure of $4EP^-$ and $4CP^-$

High-resolution photoelectron data were reported previously for $4CP^-$, and the EA of $4CP$ was measured accurately as 3.0906 eV

($24\,927\text{ cm}^{-1}$).⁴⁶ In the current study, we measured the spectrum of $4CP^-$ at a high photon energy of 266 nm, as compared with that of $4EP^-$ in Fig. 1. Except for the fact that $4CP^-$ has higher electron binding energies due to the stronger electron withdrawing effect of the $-CN$ group, the two spectra are almost identical. Both exhibit a ground state band (X) and an excited state band (A). The separation between the two bands and the Franck–Condon profiles of the two bands are similar in both spectra. The spectral similarity between the two anions indicates their similar electronic structure. The highest occupied molecular orbital (HOMO) and the HOMO-1 of the two systems are shown in Fig. S1. The two valence orbitals look almost exactly the same. The HOMO is a π orbital, corresponding to the ground state band X; the HOMO-1, mainly a σ -type orbital involving O–C antibonding interactions, corresponds to the excited state band A in each case. The separation between bands A and X, 1.050 eV for $4EP$ and 0.915 eV for $4CP$, represents the excitation energy of the first excited state of the respective neutral radicals.

To better resolved the Franck–Condon profile in the ground state band of $4EP^-$, we measured its spectrum at 355 nm, as shown in Fig. 2. The Franck–Condon factors were calculated for the ground state detachment transition using Franck–Condon (FC)-LAB2,⁷⁵ as represented by the vertical lines in Fig. 2. The geometry optimization and vibrational frequency calculations were done at the B3LYP level for the Franck–Condon factor calculation, which revealed that the most active mode in the photoelectron spectrum is ν_{13} , an in-plane C–C stretching mode (Fig. S2). The Franck–Condon active mode is consistent with the nature of the HOMO (Fig. S1), which involves C–C antibonding interactions within the phenyl ring. The previous study of $4CP^-$ showed that its ground state photoelectron band involves the same C–C stretching mode.⁴⁶ The angular distributions of the ground state transition in both $4EP^-$ and $4CP^-$ exhibit $s + d$ wave characters with photoelectrons mainly distributed perpendicularly to the direction of the laser polarization, consistent with the π character of the HOMO.

B. High-resolution PES of $4EP^-$ and the EA of $4EP$

To accurately determine the EA of $4EP$ and better resolve the vibrational structures, we took photoelectron images at several low photon energies, as shown in Fig. 3. At 464.73 nm (2.6679 eV or $21\,518\text{ cm}^{-1}$), six vibrational peaks (labeled 0_0^0 , A, C, D, E, and F) are resolved for the ground electronic state of $4EP$ [Fig. 3(c)]. The first intense peak, labeled 0_0^0 , denotes the detachment transition from

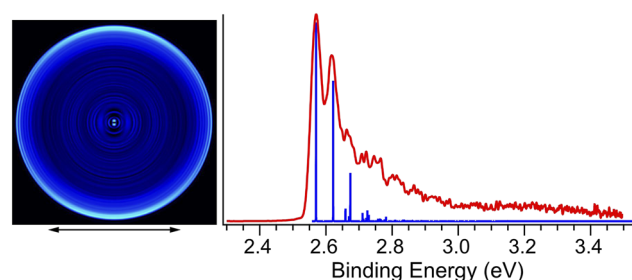


FIG. 2. Photoelectron image and spectrum of $4EP^-$ at 355 nm (3.496 eV). The calculated Franck–Condon factors are given as vertical lines. The double arrow below the image represents the laser polarization.

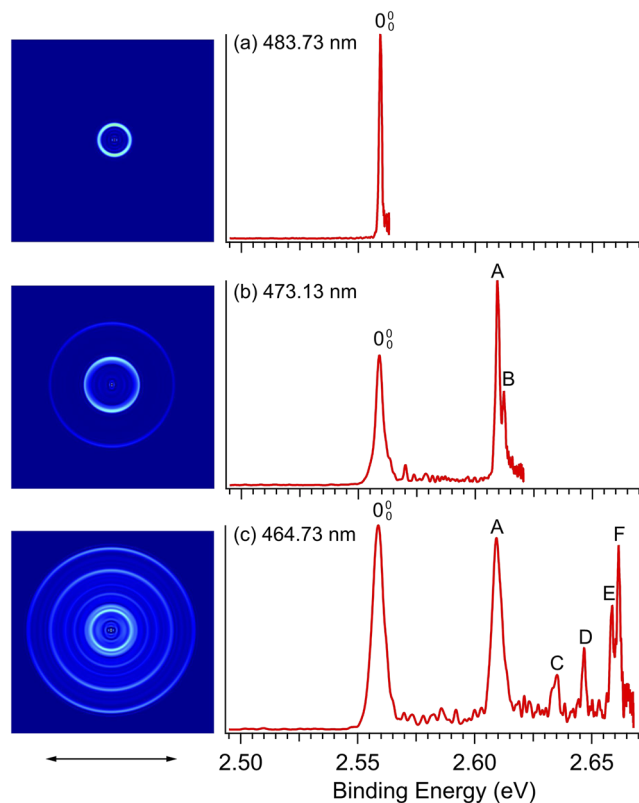


FIG. 3. Photoelectron images and spectra of $4EP^-$ at (a) 483.73 nm (2.5631 eV), (b) 473.13 nm (2.6205 eV), and (c) 464.73 nm (2.6679 eV). The double arrow below the images indicates the direction of the laser polarization.

the vibrational ground state of $4EP^-$ to that of neutral $4EP$ and defines the EA of $4EP$. Peaks A–F represent the excited vibrational levels of neutral $4EP$. At 473.13 nm (2.6205 eV or $21\,136\text{ cm}^{-1}$), one additional vibrational peak (labeled B) is resolved on the high

binding energy side of peak A [Fig. 3(b)]. At 483.73 nm (2.5631 eV or $20\,673\text{ cm}^{-1}$), which is slightly above the detachment threshold [Fig. 3(a)], we obtained the best resolved 0_0^0 transition, resulting in the most accurate measurement for the EA of $4EP$ as $20\,643 \pm 6\text{ cm}^{-1}$ ($2.5594 \pm 0.0007\text{ eV}$). The electron binding energies of all the observed vibrational peaks, their shifts from peak 0_0^0 , and their assignments are summarized in Table I. Additional vibrational peaks from rPES (*vide infra*) are also given in Table I. The spectral assignments are assisted by the PDS to be presented later. Specifically, the strong peak A corresponds to the $v = 1$ level of the most Franck–Condon active ν_{13} mode.

C. Photodetachment spectroscopy of $4EP^-$

Our calculations estimated a dipole moment of 3.8 D for the $4EP^-$ radical, suggesting that the $4EP^-$ anion should possess a DBS as an electronically excited state below its detachment threshold. To search for the DBS, we conducted PDS by scanning the detachment laser around the threshold while monitoring the total electron yield in the energy range from $20\,300\text{ cm}^{-1}$ (2.5169 eV) to $21\,415\text{ cm}^{-1}$ (2.6551 eV), as shown in Fig. 4. The arrow at $20\,643\text{ cm}^{-1}$ indicates the detachment threshold measured from the high-resolution PES discussed above (Fig. 3), coinciding with the prompt appearance of continuous photodetachment signals with increasing photon energies, as expected. Several sharp peaks were observed (0–6), evidencing the existence of a DBS. Peak 0 below the threshold should correspond to the ground state of the DBS, and the above-threshold peaks 1–6 represent the vibrational levels of the DBS, i.e., vibrational Feshbach resonances. The spectrum in Fig. 4 was taken with a scan step of 0.1 nm. For all the observed peaks, additional PDS data were taken at a step size of 0.01 nm in order to measure the excitation energies more accurately. The ground state of the DBS (peak 0) at $20\,567\text{ cm}^{-1}$ was observed as a result of R2PD. The energy difference between the detachment threshold and peak 0 defines the binding energy of the DBS to be $76 \pm 5\text{ cm}^{-1}$. The continuous above-threshold signals in Fig. 4 represent contributions from single-photon nonresonant detachment processes. The six above-threshold peaks in Fig. 4 are due to single-photon excitation to the

TABLE I. Observed vibrational peaks in the PES (capital letters) and rPES (lower case letters) of $4EP^-$, with their binding energies in both eV and cm^{-1} , shifts relative to the 0–0 transition, and their assignments. The theoretical frequencies of $4EP$ are also given for comparison (see Fig. S2 and Table S1).

Observed peak	Binding energy (eV) ^a	Binding energy (cm^{-1}) ^a	Shift (cm^{-1})	Assignment	Theoretical frequency (cm^{-1})
0_0^0	2.5594(7)	20 643(6)	0	Neutral ground state	
A	2.6094(9)	21 046(7)	403	13^1	418
B	2.6122(5)	21 069(4)	426	23^2	440
C	2.6345(7)	21 249(6)	606	33^1	631
D	2.6468(9)	21 348(7)	705	$12^1/21^1 24^2/24^2 34^1/13^1 23^1 24^1$	717/720/717/729
E	2.6588(11)	21 445(9)	802	13^2	836
F	2.6615(8)	21 466(6)	823	$13^1 23^2$	858
a	2.5700(14)	20 728(11)	85	24^1	91
b	2.5854(8)	20 853(6)	210	23^1	220
c	2.6206(9)	21 137(7)	494	$13^1 24^1$	509
d	2.6242(8)	21 166(6)	523	$21^1/34^1$	538/535
e	2.6393(6)	21 287(5)	644	$16^1 36^2$	677

^aThe numbers in parentheses indicate the experimental uncertainties in the last digit.

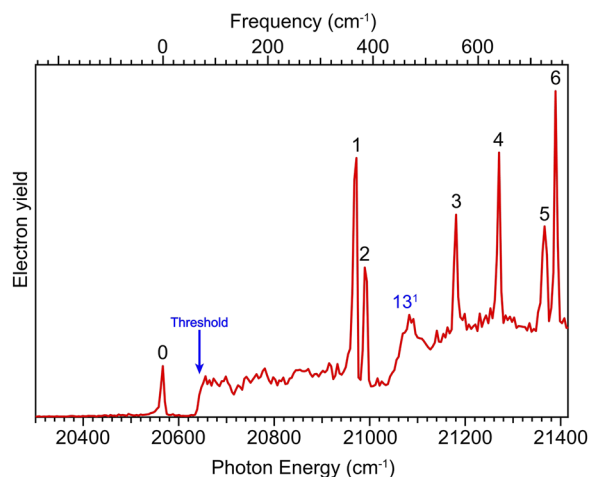


FIG. 4. Photodetachment spectrum of $4EP^-$. The arrow at $20\,643\text{ cm}^{-1}$ indicates the detachment threshold. Peak 0 below the detachment threshold represents the ground vibrational level of the DBS. The six above-threshold peaks (also known as vibrational Feshbach resonances) correspond to vibrational levels of the DBS. The broad peak at about $21\,060\text{ cm}^{-1}$ is due to the $v = 1$ vibrational level of the ν_{13} mode of $4EP^-$ (peak A in the photoelectron spectra in Fig. 3).

vibrational levels of the DBS, followed by vibrational autodetachment. The wavelengths, photon energies, and assignments of the DBS vibrational peaks are given in Table II.

A broad peak was observed around $21\,060\text{ cm}^{-1}$, beyond which an increased level of continuous signals was observed, indicating the opening of a new detachment channel. The broad peak coincides with peak A in the photoelectron spectra (Fig. 3), i.e., the $v = 1$ level of the most Franck–Condon-active ν_{13} mode. A step is expected in the PDS when a new detachment channel is opened. The broad peak corresponding to 13^1 shows a Fano line shape,⁷⁶ possibly due to the interference between the $v = 0$ and $v = 1$ detachment channels.

D. Resonant photoelectron spectroscopy of $4EP^-$

Resonant photoelectron spectra can be obtained by measuring photoelectron images at detachment photon energies corresponding to the Feshbach resonances in Fig. 4, as presented in Fig. 5. Comparing these spectra to the data in Fig. 3, we can readily

see that one or more vibrational peaks are enhanced (labeled in bold face), as well as additional peaks that are not observed in the nonresonant photoelectron spectra, either because of their low Franck–Condon factors or because they are Franck–Condon inactive. Thus, all the resonant photoelectron spectra in Fig. 5 are highly non-Franck–Condon. All the observed peaks, their binding energies, energy shifts relative to the 0–0 transition, and their assignments are also given in Table I.

E. R2PD photoelectron imaging of $4EP^-$ and comparison with that of $4CP^-$

1. R2PD photoelectron imaging of $4EP^-$

By tuning the detachment laser to the bound vibrational ground state of the DBS (peak 0 in Fig. 4), we obtained the R2PD photoelectron image and spectrum of $4EP^-$, as shown in Fig. 6. The R2PD data in Fig. 6 contain two features: (1) a low binding energy peak marked as “DBS” and (2) a high energy cutoff marked as “ S_0 .” The low binding energy peak represents a R2PD process in which the first photon excited the anion to the bound $v = 0$ level of the DBS and the second photon within the same laser pulse detached the dipole-bound electron, producing high kinetic energy photoelectrons, i.e., the outermost ring in the image (Fig. 6). The photoelectron image exhibits a p -wave distribution, as expected from the s -like DBS orbital. The most prominent feature in the R2PD image is the bright center spot, corresponding to strong threshold electrons (labeled “ S_0 ” in the converted spectrum). The low binding energy “DBS” signal was the only feature expected if the DBS ground state has a lifetime exceeding the detachment laser pulse length (5 ns). The strong high binding energy feature suggests that relaxation processes have taken place from the DBS within 5 ns upon absorption of the first photon, producing rovibrationally excited $4EP^-$ in its ground electronic state (S_0). The second photon within the same laser pulse then detached the rovibrationally excited $4EP^-$ from S_0 (those with more than 76 cm^{-1} excitation energies), giving rise to the strong threshold electrons. The sharp threshold behavior suggests that the second photon only detached rotationally excited levels of $4EP^-$.

2. R2PD photoelectron imaging of $4CP^-$

To compare with $4EP^-$, we also measured the R2PD photoelectron image and spectrum for the bound $v = 0$ level of the QBS in $4CP^-$ (Fig. 7), which was not investigated previously.⁴⁶ In

TABLE II. Observed DBS vibrational peaks for $4EP^-$, their wavelengths, energies in cm^{-1} , shifts relative to the ground vibrational level, assignments, and comparison with the computed frequencies.

Peak	Wavelength (nm)	Photon energy (cm^{-1}) ^a	Shift (cm^{-1})	Assignment	Theoretical frequency (cm^{-1})
0	486.22	20 567(5)	0	Ground state DBS	
1	476.89	20 969(5)	402	13^1	418
2	476.39	20 991(5)	424	23^2	440
3	472.20	21 177(5)	610	33^1	631
4	470.14	21 270(5)	703	$12^1/21^1 24^2/24^2 34^1/13^1 23^1 24^1$	717/720/717/729
5	468.01	21 367(5)	800	13^2	836
6	467.52	21 389(5)	822	$13^1 23^2/23^1 33^1/16^1 24^2 36^2$	858/851/859

^aThe numbers in parentheses indicate the experimental uncertainties in the last digit.

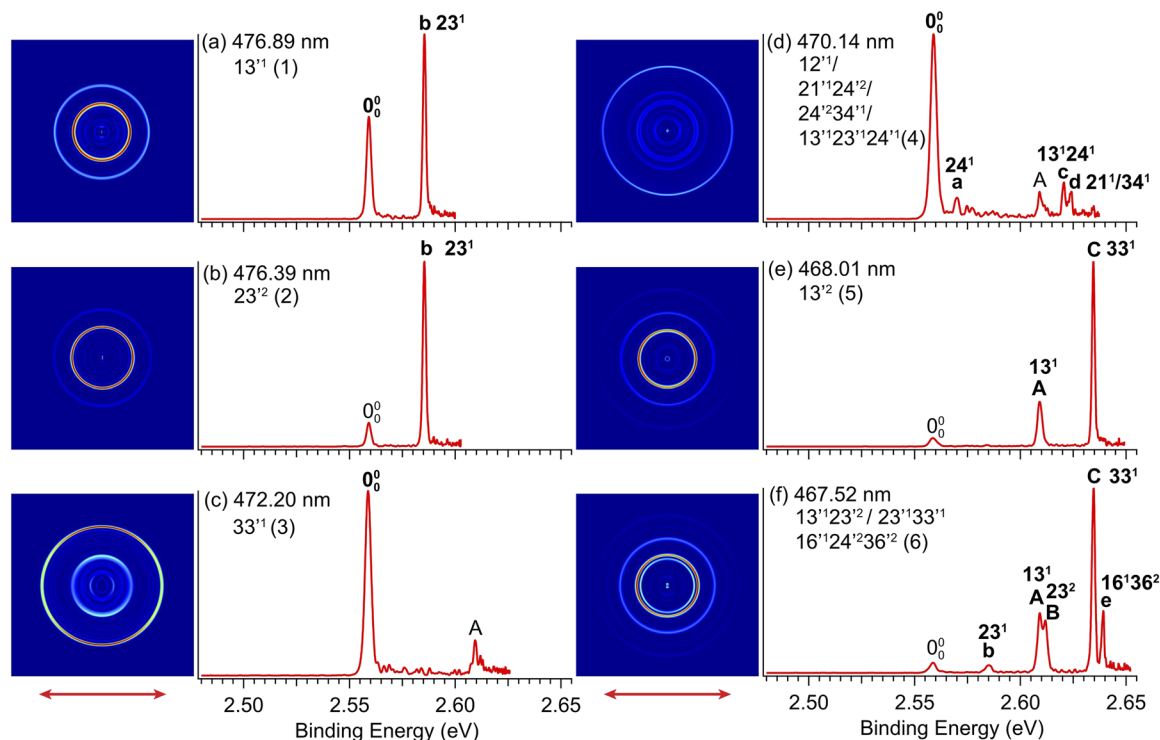


FIG. 5. Resonant photoelectron images and spectra of $4EP^-$, corresponding to peaks 1–6 in Fig. 4 at (a) 476.89 nm (2.5998 eV), (b) 476.39 nm (2.6026 eV), (c) 472.20 nm (2.6256 eV), (d) 470.14 nm (2.6371 eV), (e) 468.01 nm (2.6492 eV), and (f) 467.52 nm (2.6519 eV). The enhanced peaks are labeled in bold face. The wavelengths and the assignments of the DBS are also given, as well as the resonant peak numbers in parentheses.

addition to the expected low binding energy feature (“QBS”), we also observed high binding energy signals, suggesting that decay has also occurred from the bound QBS vibrational level to S_0 of $4CP^-$ within the 5 ns laser pulse upon absorption of the first photon. The p -wave distribution of the “QBS” feature (the outer ring in the image) is also consistent with the s -type orbital for the QBS in $4CP^-$.

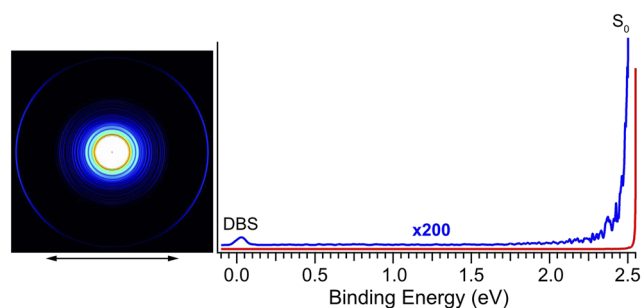


FIG. 6. R2PD photoelectron image and spectrum of $4EP^-$ via the ground vibrational level of the DBS at 486.22 nm ($20\,567\text{ cm}^{-1}$, 2.5500 eV) corresponding to peak 0 in Fig. 4. The double arrow below the image represents the laser polarization. The low binding energy peak marked as “DBS” is produced by sequential R2PD. The high binding energy feature marked as “ S_0 ” indicates decay from the DBS has taken within the 5 ns laser pulse, and the signals come from photodetachment of highly rotationally excited $4EP^-$ in its ground electronic state (S_0) by the second photon.

However, the high binding energy signals in the R2PD spectrum of $4CP^-$ contain surprising fine features (α , β , γ , δ), as shown in the inset of Fig. 7. The high binding energy part of the R2PD spectrum for $4CP^-$ is compared with that of $4EP^-$ in Fig. 8. The threshold signals and the resolved vibrational features suggest that both rotational and vibrational excited states were populated in S_0 due to the decay from the QBS of $4CP^-$. The threshold feature in the R2PD spectrum of $4CP^-$ should come from rotationally excited states of the ground vibrational level, whereas the four distinct peaks should come from detachment of vibrationally excited states in S_0 by the second photon. We calculated the vibrational frequencies of $4CP^-$ (see Table S2 and Fig. S3), which allowed us to assign these four peaks (Table S3). It turns out that they correspond to ν_{22a} , ν_{33a} , $2\nu_{22a}$, and ν_{21a} , respectively (the subscript “a” is used here to denote the vibrational levels of the $4CP^-$ anion), which are the first four lowest vibrational levels of $4CP^-$. In other words, the relaxation from the QBS populated both rotationally and vibrationally excited states in S_0 of $4CP^-$, whereas mainly rotationally excited states were produced from the decay of the DBS in $4EP^-$.

IV. DISCUSSION

A. Comparison of the photoelectron and photodetachment spectrum of $4EP^-$

It is known that the highly diffuse nonvalence-bound electron has very little effect to the structures of the neutral cores in

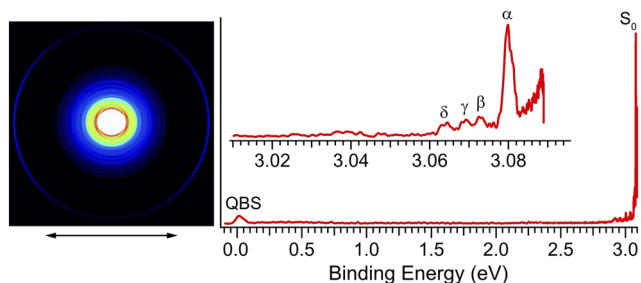


FIG. 7. R2PD photoelectron image and spectrum of $4CP^-$ via the ground vibrational level of the QBS at 401.38 nm ($24\,914\text{ cm}^{-1}$, 3.0889 eV). The inset shows the fine features resolved for the high binding energy signals.

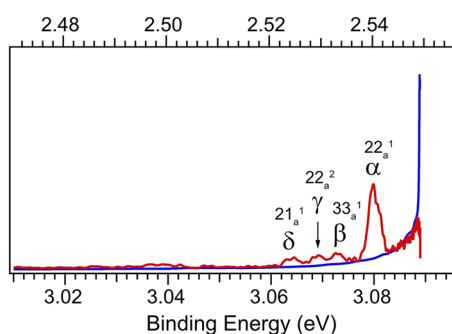


FIG. 8. Comparison of the high binding energy part of the R2PD photoelectron spectra of $4CP^-$ (red, bottom axis) and $4EP^-$ (blue, upper axis). The assignments of the four vibrational peaks in the spectrum of $4CP^-$ are shown.

nonvalence states. In the case of C_2P^- , it was found that the dipole-bound electron was not even spin-coupled with the unpaired electrons in the C_2P molecular core.⁷⁷ To illustrate the similarity of the neutral core of the DBS in $4EP^-$ and the $4EP$ neutral radical, we compare the photodetachment spectrum and the nonresonant photoelectron spectrum on the same energy scale in Fig. 9, where the photoelectron spectrum at 464.73 nm [Fig. 3(c)] is overlaid on top of the photodetachment spectrum (Fig. 4) by aligning the 0_0^0 transition of the former with the DBS ground state. It can be readily seen that all the vibrational peaks and their relative intensities agree with each other in the two spectra, except that the photodetachment spectrum has higher resolution. This spectral resemblance between PES and PDS provides vivid evidence that the structure of the neutral core in the DBS of $4EP^-$ and that of the neutral $4EP$ radical are identical. The similarity between PES and PDS provides the basis to use photodetachment spectra of nonvalence states to obtain more accurate vibrational information for the neutral species. We have shown that combining PDS and rPES can yield substantially more vibrational information for the underlying neutral species.^{52–54} It should also be pointed out that if we align the 0_0^0 transition of the PES with the detachment threshold in the photodetachment spectrum, peak A would align exactly with the broad feature (13^1) around $21\,060\text{ cm}^{-1}$ in Fig. 9.

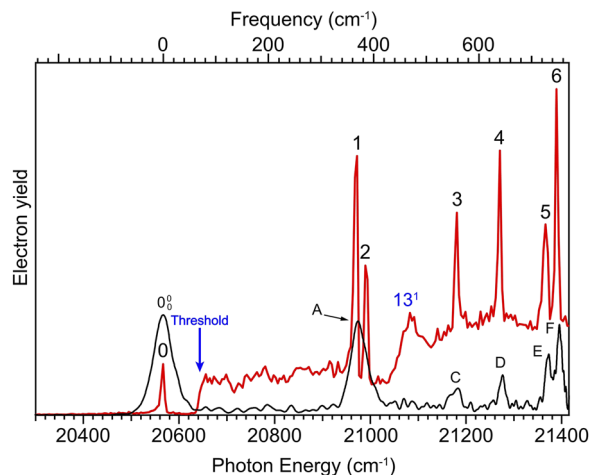


FIG. 9. Comparison of the nonresonant photoelectron spectrum (black) at 464.73 nm from Fig. 3(c) with the photodetachment spectrum (red) from Fig. 4. The photoelectron spectrum is red-shifted by 76 cm^{-1} to line up the 0_0^0 transition with the ground vibrational level of the DBS.

B. Resonant PES via the vibrational Feshbach resonances of $4EP^-$

High-resolution and resonant photoelectron spectra of $4CP^-$ were reported previously.⁴⁶ Here, we discuss the resonant photoelectron spectra of $4EP^-$ presented in Fig. 5. Resonant photoelectron spectra consist of signals from two detachment processes: (1) the nonresonant detachment process and (2) the resonant excitation to a vibrational level of the DBS followed by vibrational autodetachment, which often dominates rPES because of the much larger resonant optical excitation cross sections. Since the structures of the DBS and the corresponding neutral are almost identical, the vibrational autodetachment follows the harmonic oscillator selection rule, $\Delta v = -1$,^{55,56} i.e., only one vibrational quantum can be coupled to the DBS electron during autodetachment. Violation of the $\Delta v = -1$ propensity rule can happen as a result of the anharmonic effect and has been observed often for low-frequency bending vibrations. Thus, one or more vibrational final states are enhanced in the resonant photoelectron spectra. Because of the large optical excitation cross sections, vibrational transitions with low Franck–Condon factors or even Franck–Condon inactive modes can be observed in PDS, allowing significantly more vibrational information to be obtained in rPES than conventional PES, which only allows Franck–Condon active modes to be observed.

Using the $\Delta v = -1$ propensity rule, the comparison between the PES and PDS in Fig. 9, and the calculated frequencies of $4EP$ (Table S1), we can assign all the vibrational levels of the DBS observed in Fig. 4 as given in Table II and the rPES data in Fig. 5 as shown in Table I. Peak 1 is due to excitation to 13^1 of the DBS (the prime ' is used to designate the vibrational modes of the DBS, even though the structures of the DBS and the neutral final states are practically the same). Autodetachment from the 13^1 DBS level should enhance the 0_0^0 peak in rPES, following the $\Delta v = -1$ propensity rule. However, the Franck–Condon inactive 23^1 final state is also observed prominently in the rPES data at peak 1 [Fig. 5(a)] due to the overlap of

peak 1 and the rotational tail of peak 2. The latter is due to excitation to 23^2 , which leads to the strong 23^1 final state in the rPES data [Fig. 5(b)]. Peaks 1 and 2 correspond to peaks A and B, respectively, in the nonresonant PES data (see Fig. 9), which are barely resolved in Fig. 3(b). The ν_{23} mode is an out-of-plane bending mode (Fig. S2), and only even quanta are symmetry-allowed in PES. Thus, the 23^1 final state is not observed in the PES data in Fig. 3. Peak 3 corresponds to excitation to the 33^1 DBS level, which led to strong enhancement of the 0_0^0 transition in the rPES [Fig. 5(c)].

Peak 4 in the PDS is due to excitation to ν_{12}^1 , resulting in the strong enhancement of the 0_0^0 transition in the rPES data [Fig. 5(d)]. The ν_{12} mode is Franck–Condon active and is also observed in the nonresonant spectrum [peak D in Fig. 3(c)]. However, the rPES data in Fig. 5(d) also display three weak new peaks, *a*, *c*, and *d* (Table I), whose origins are more complicated and can only be assigned tentatively. Peak *a* is 85 cm^{-1} above the 0_0^0 transition, corresponding to the lowest frequency bending mode (ν_{24} , Fig. S2) with a computed frequency of 91 cm^{-1} . Similar weak low frequency excitations have been observed previously in rPES and were attributed to inelastic scattering by the outgoing electrons of the intense 0_0^0 transition.⁷⁸

Peak *c* can be assigned to the $13^1 24^1$ final state due to autodetachment from the $13^1 23^1 24^1$ DBS level. Peak *d* can be assigned to either 21^1 or 34^1 because the computed frequency of ν_{21} (538 cm^{-1}) and ν_{34} (535 cm^{-1}) (Table S1) is nearly identical. It can be due to weak excitation to either the $21^1 24^2$ or $24^2 34^1$ DBS level followed by $\Delta v = -2$ autodetachment from the ν_{24}^1 mode. The rPES data from peak 5 [Fig. 5(e)] are due to excitation to the 13^2 DBS level, leading to the enhancement of the 13^1 final state. The enhancement of peak C in Fig. 5(e) is likely due to the overlap of peak 5 with the rotational tail of peak 6, similar to the resonant spectrum of Fig. 5(a) discussed above. The rPES data from peak 6 are also complicated with several overlapping DBS levels. The enhancement of 33^1 and 23^1 suggests a DBS level of $23^1 33^1$, whereas the enhancement of 13^1 and 23^2 comes from excitation to the $13^1 23^2$ DBS level. The addition peak *e* (644 cm^{-1} above the 0_0^0 transition) may be assigned tentatively to the $16^1 36^2$ final state due to excitation to the $16^1 24^2 36^2$ DBS level. A schematic energy level diagram showing all the DBS vibrational levels and their autodetachment to the relevant neutral final states is shown in Fig. 10, where the EA of 4EP and the binding energy of the DBS are also given.

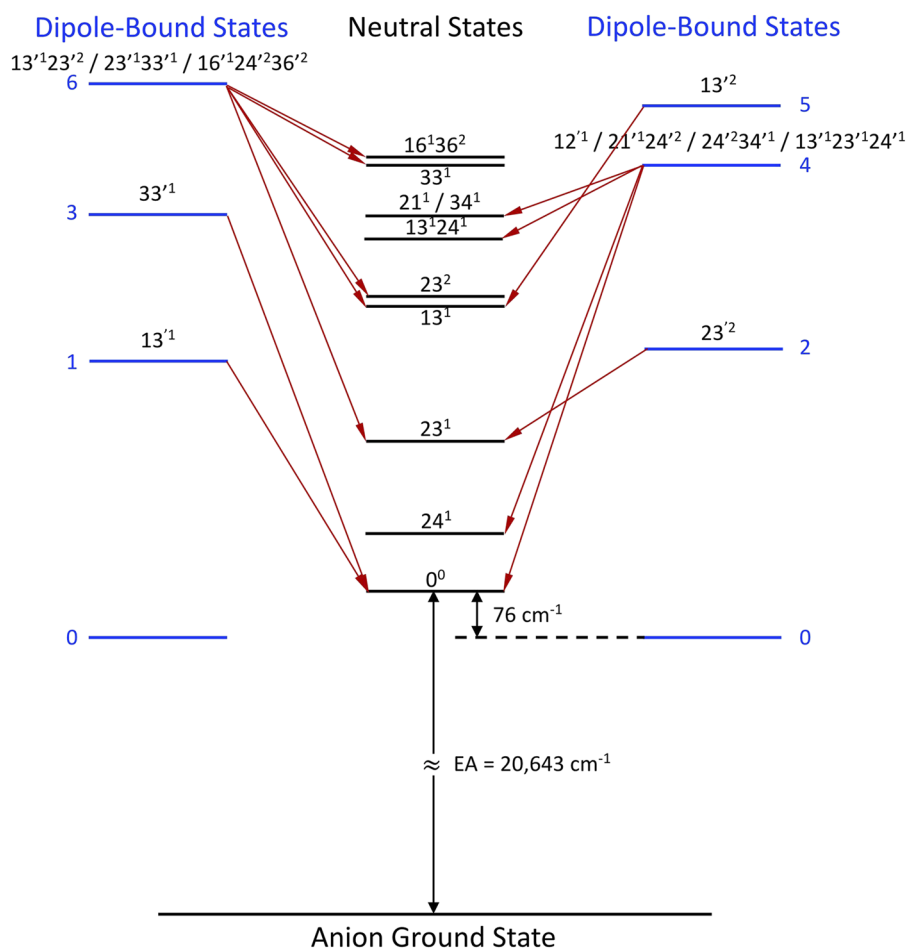


FIG. 10. Schematic energy level diagram for autodetachment from the DBS vibrational levels of 4EP^- to the related neutral final states, corresponding to the six resonant PE spectra shown in Fig. 5.

C. R2PD PES and relaxations from the nonvalence excited states of $4EP^-$ and $4CP^-$

The different R2PD photoelectron spectra of $4EP^-$ and $4CP^-$ are surprising, suggesting different decay mechanisms from the different nonvalence states. Relaxations from the bound levels of nonvalence excited states have been observed in almost all the anionic systems that we have studied, always manifested as low kinetic energy features in the center of the R2PD images. The decay can occur in two steps: (1) internal conversion (IC) from the nonvalence excited states to the manifold of highly excited rovibrational levels on the potential energy surface of S_0 and (2) intramolecular vibrational redistribution (IVR) and relaxation to the lower rovibronic states of S_0 via radiative processes. The two decay steps are shown schematically in Fig. 11 for $4CP^-$ and $4EP^-$. These decay processes usually yield broad and featureless tails on the high binding energy side of the R2PD photoelectron spectra, reminiscent of rovibrational hot bands. What is surprising is the observation of distinct

vibrational peaks in the R2PD spectrum of $4CP^-$ (Fig. 7) and the sharp threshold feature in the case of $4EP^-$ (Fig. 6).

The sharp “ S_0 ” feature in the R2PD spectrum of $4EP^-$ implies that the second photon only detached highly rotationally excited states ($>76\text{ cm}^{-1}$) from the vibrational ground state of S_0 , as shown schematically in Fig. 11(b). In other words, the decay from the DBS of $4EP^-$ produced highly rotationally excited states, but negligible vibrationally excited states. P and R branches were observed for the ground vibrational level of the DBS, but identical R2PD spectra were observed, regardless whether the detachment laser was set at the P or R branch (Fig. S4). Such a sharp threshold detachment feature due to rotational autodetachment was observed previously in 4-florophenoxide,³⁰ which has a DBS with a very small binding energy of 8 cm^{-1} . Thus, at a rotational temperature of $\sim 30\text{ K}$ in our cryogenic ion trap, there were sufficient rotationally excited anions ($>8\text{ cm}^{-1}$) to produce a sharp threshold feature at each vibrational level of the DBS in rPES due to excitation from the rotationally excited anions. In the case of $4EP^-$, our observation suggests that

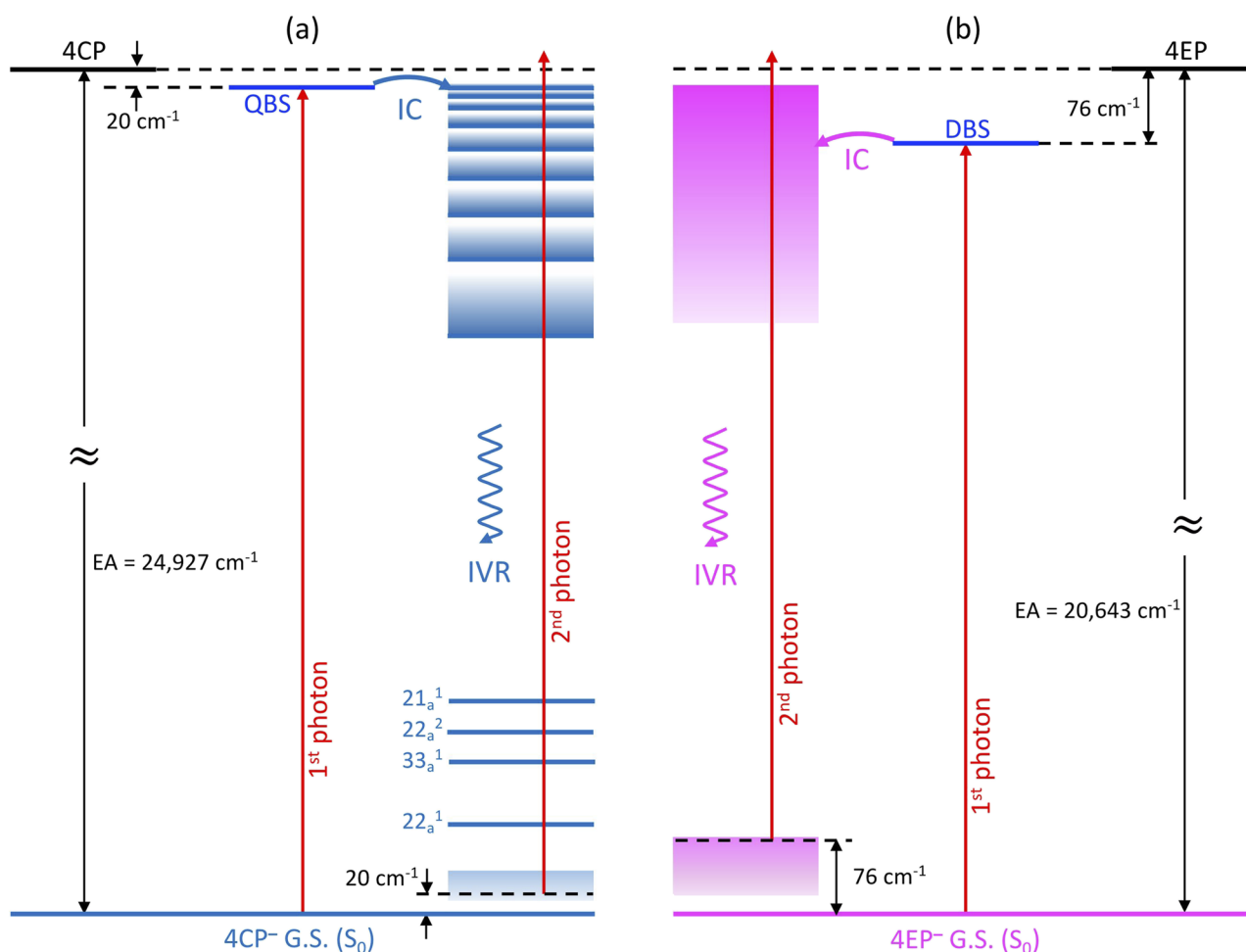


FIG. 11. Schematic diagrams illustrating the decay processes from the nonvalence excited state to S_0 and the origins of the high binding energy features in the R2PD of $4EP^-$ (a) and $4CP^-$ (b). Note the population of rovibrational levels in S_0 from the QBS of $4CP^-$, but only rotational levels from the DBS of $4EP^-$. IC = internal conversion; IVR = intramolecular vibrational redistribution.

much higher rotationally excited states were populated due to the decay from the bound vibrational level of the DBS, as illustrated schematically in Fig. 11(b).

On the other hand, the decay from the QBS of 4CP^- appeared to have populated the four lowest vibrational levels in S_0 , which were then detached by the second photon during R2PD, as schematically shown in Fig. 11(a). IVR is generally a very fast process,^{79–82} but the radiative lifetimes of the four lowest vibrational levels of 4CP^- could be long, in particular because of its very small dipole moment. One interesting question is why there seemed to be much lower population of rotational states in the decay of the QBS, as compared with the DBS in 4EP^- (Fig. 8). The rotational population is represented by the near threshold feature, as readily seen in Fig. 8. We noted that the rotational population following the decay from the QBS of 4CP^- is related to the original rotational excitation of the anion, as shown in Fig. 12. We also observed *P* and *R* branches in the transition to the ground state of the QBS (inset of Fig. 12). For the R2PD spectrum at the lower energy side of the *P* branch, only vibrational populations were observed in the decay to S_0 with little rotational tail (the bottom light blue spectrum in Fig. 12). On the other hand, in the R2PD spectrum at the higher energy side of the *R* branch, significantly more rotational populations were produced by the decay from the QBS (the top yellow-green spectrum in Fig. 12). The ratio of the rotational vs vibrational population as a function of photon energy across the rotational profile is quantitatively shown in Fig. S5. Thus, there seems to be a relationship between the initial population of rotational energy following the IC and the eventual vibrational population in S_0 after IVR and other radiative processes. Even though the mechanisms of the IC are not known, it seems that the IC from the DBS of 4EP^- leads to highly rotationally excited states that suppresses vibrational populations in S_0 following the IVR and radiative processes, whereas the IC from the QBS of 4CP^- leads to much less rotational excitations in the upper manifold of S_0 , resulting in significant vibrational population following IVR and radiative relaxation. The current work provides quantitative experimental observations to test future theoretical models to treat the decay processes from nonvalence excited states to valence-bound states, which are important to understand anion formation via electron capturing by nonvalence interactions.

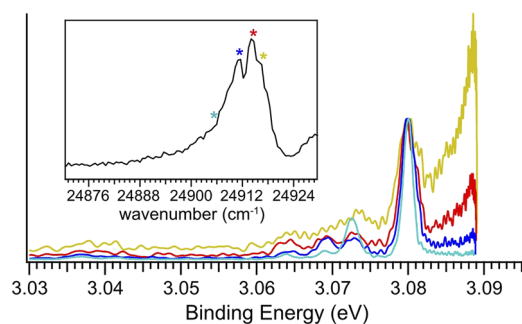


FIG. 12. R2PD photoelectron spectra of 4CP^- at different positions across the rotational profile of the bound $v = 0$ level of its QBS: $24\,906\text{ cm}^{-1}$ (light blue), $24\,911\text{ cm}^{-1}$ (dark blue), $24\,914\text{ cm}^{-1}$ (red), and $24\,917\text{ cm}^{-1}$ (yellow-green). The inset displays a high-resolution photodetachment spectrum (0.01 nm/step) of the $v = 0$ level of the QBS; the color-coded * signs indicate the four detachment laser wavelengths used in the R2PD experiment.

V. CONCLUSION

In conclusion, we report a comparative study of a dipole-bound and a quadrupole-bound excited state in a pair of similar and isoelectronic anions, 4-ethynylphenoxide ($\text{HCC-C}_6\text{H}_4\text{O}^-$) and 4-cyanophenoxide ($\text{NC-C}_6\text{H}_4\text{O}^-$). High-resolution nonresonant and resonant photoelectron imaging and photodetachment spectroscopy were conducted for cryogenically cooled 4EP^- . The electron affinity of the 4EP^- radical is measured to be $20\,643 \pm 6\text{ cm}^{-1}$ ($2.5594 \pm 0.0007\text{ eV}$). The photodetachment spectrum revealed a DBS for 4EP^- 76 cm^{-1} below its detachment threshold, as well as six vibrational Feshbach resonances, which allowed six non-Franck–Condon resonant photoelectron spectra to be obtained. The electronic structure of 4EP^- was found to be nearly identical to the isoelectronic 4CP^- , which was found to possess a QBS 20 cm^{-1} below its detachment threshold previously. Even though the structures and electronic properties of 4EP^- and 4CP^- were found to be similar, R2PD photoelectron spectra via the bound $v = 0$ level of their nonvalence excited states were found to be very different. Both nonvalence excited states were observed to decay to the S_0 states of the respective anions within the 5 ns detachment laser pulse, but the decay mechanisms appeared to be different. The relaxation from the DBS of 4EP^- preferentially produced highly rotationally excited anions in S_0 , whereas the decay from the QBS of 4CP^- seems to produce mainly vibrationally excited anions in S_0 . The current study provides insight into the relaxation processes from the bound vibrational levels of nonvalence excited states to the anionic ground states. The differences observed for the relaxation processes from the DBS and QBS are intriguing. It would be interesting to investigate in future studies if these behaviors are general for different types of nonvalence excited states.

SUPPLEMENTARY MATERIAL

See the [supplementary material](#) for the valence molecular orbitals of 4-ethynylphenoxide and 4-cyanophenoxide, vibrational analyses for neutral 4-ethylphenoxy and 4-cyanophenoxide, R2PD photoelectron spectra of 4-ethynylphenoxide at two-photon energies, the ratio of the rotational vs vibrational population following relaxation from the quadrupole-bound excited state of 4-cyanophenoxide as a function of photon energy, and the binding energies and assignments of the observed vibrational features in the R2PD photoelectron spectra of 4-cyanophenoxide.

ACKNOWLEDGMENTS

We would like to thank Dr. G. Z. Zhu, Dr. Y. Liu, and Professor T. Sommerfeld for helpful discussions. This work was supported by the Department of Energy, Office of Basic Energy Sciences, Chemical Sciences, Geosciences, and Biosciences Division under Grant No. DE-SC0018679. The calculation was performed using computational resources and services provided by CCV of Brown University.

The authors have no conflicts to disclose.

DATA AVAILABILITY

The data that support the findings of this study are available from the corresponding authors upon reasonable request.

REFERENCES

- ¹J. Simons, *J. Phys. Chem. A* **112**, 6401–6511 (2008).
- ²C. Desfrancois, H. Abdoul-Carime, and J.-P. Schermann, *Int. J. Mod. Phys. B* **10**, 1339–1395 (1996).
- ³R. N. Compton and N. I. Hammer, *Adv. Gas Phase Ion Chem.* **4**, 257–305 (2001).
- ⁴K. D. Jordan and F. Wang, *Annu. Rev. Phys. Chem.* **54**, 367–396 (2003).
- ⁵M. Gutowski, P. Skurski, A. I. Boldyrev, J. Simons, and K. D. Jordan, *Phys. Rev. A* **54**, 1906–1909 (1996).
- ⁶T. Sommerfeld, K. M. Dreux, and R. Joshi, *J. Phys. Chem. A* **118**, 7320–7329 (2014).
- ⁷K. D. Jordan and J. F. Liebman, *Chem. Phys. Lett.* **62**, 143–147 (1979).
- ⁸C. Desfrancois, Y. Bouteiller, J. P. Schermann, D. Radisic, S. T. Stokes, K. H. Bowen, N. I. Hammer, and R. N. Compton, *Phys. Rev. Lett.* **92**, 083003 (2004).
- ⁹G. Liu, S. M. Ciburowski, J. D. Graham, A. M. Buytendyk, and K. H. Bowen, *J. Chem. Phys.* **151**, 101101 (2019).
- ¹⁰Y. Liu, G.-Z. Zhu, D.-F. Yuan, C.-H. Qian, Y.-R. Zhang, B. M. Rubenstein, and L.-S. Wang, *J. Am. Chem. Soc.* **142**, 20240–20246 (2020).
- ¹¹V. G. Bezchastnov, V. P. Vysotskiy, and L. S. Cederbaum, *Phys. Rev. Lett.* **107**, 133401 (2011).
- ¹²V. K. Voora, L. S. Cederbaum, and K. D. Jordan, *J. Phys. Chem. Lett.* **4**, 849–853 (2013).
- ¹³V. K. Voora and K. D. Jordan, *J. Phys. Chem. Lett.* **6**, 3994–3997 (2015).
- ¹⁴H. Abdoul-Carime and C. Desfrancois, *Eur. Phys. J. D* **2**, 149–156 (1998).
- ¹⁵K. J. Taylor, C. Jin, J. Conceicao, L. S. Wang, O. Cheshnovsky, B. R. Johnson, P. J. Nordlander, and R. E. Smalley, *J. Chem. Phys.* **93**, 7515–7518 (1990).
- ¹⁶E. Fermi and E. Teller, *Phys. Rev.* **72**, 399–408 (1947).
- ¹⁷J. E. Turner, *Am. J. Phys.* **45**, 758–766 (1977).
- ¹⁸W. R. Garrett, *J. Chem. Phys.* **73**, 5721–5725 (1980).
- ¹⁹J. A. Stockdale, F. J. Davis, R. N. Compton, and C. E. Klots, *J. Chem. Phys.* **60**, 4279–4285 (1974).
- ²⁰C. Desfrancois, H. Abdoul-Carime, N. Khelifa, and J. P. Schermann, *Phys. Rev. Lett.* **73**, 2436–2439 (1994).
- ²¹N. I. Hammer, K. Diri, K. D. Jordan, C. Desfrancois, and R. N. Compton, *J. Chem. Phys.* **119**, 3650–3660 (2003).
- ²²G. Liu, S. M. Ciburowski, J. D. Graham, A. M. Buytendyk, and K. H. Bowen, *J. Chem. Phys.* **153**, 044307 (2020).
- ²³R. L. Jackson, A. H. Zimmerman, and J. I. Brauman, *J. Chem. Phys.* **71**, 2088–2094 (1979).
- ²⁴R. L. Jackson, P. C. Hiberty, and J. I. Brauman, *J. Chem. Phys.* **74**, 3705–3712 (1981).
- ²⁵K. R. Lykke, R. D. Mead, and W. C. Lineberger, *Phys. Rev. Lett.* **52**, 2221–2224 (1984).
- ²⁶R. D. Mead, K. R. Lykke, W. C. Lineberger, J. Marks, and J. I. Brauman, *J. Chem. Phys.* **81**, 4883–4892 (1984).
- ²⁷K. Yokoyama, G. W. Leach, J. B. Kim, W. C. Lineberger, A. I. Boldyrev, and M. Gutowski, *J. Chem. Phys.* **105**, 10706–10718 (1996).
- ²⁸C. E. H. Dessent, J. Kim, and M. A. Johnson, *Acc. Chem. Res.* **31**, 527–534 (1998).
- ²⁹H.-T. Liu, C.-G. Ning, D.-L. Huang, P. D. Dau, and L.-S. Wang, *Angew. Chem., Int. Ed.* **52**, 8976–8979 (2013).
- ³⁰C.-H. Qian, G.-Z. Zhu, and L.-S. Wang, *J. Phys. Chem. Lett.* **10**, 6472–6477 (2019).
- ³¹D. B. Dao and R. Mabbs, *J. Chem. Phys.* **141**, 154304 (2014).
- ³²K. J. Mascariolo, A. M. Gardner, and M. C. Heaven, *J. Chem. Phys.* **143**, 114311 (2015).
- ³³J. N. Bull, J. T. Buntine, M. S. Scholz, E. Carrascosa, L. Giacomozzi, M. H. Stockett, and E. J. Bieske, *Faraday Discuss.* **217**, 34–46 (2019).
- ³⁴Y. Lu, R. Tang, and C. Ning, *J. Phys. Chem. Lett.* **12**, 5897–5902 (2021).
- ³⁵P. D. Burrow, G. A. Gallup, A. M. Scheer, S. Denifl, S. Ptasinska, T. Märk, and P. Scheier, *J. Chem. Phys.* **124**, 124310 (2006).
- ³⁶B. Boudaiffa, P. Cloutier, D. Hunting, M. A. Huels, and L. Sanche, *Science* **287**, 1658–1660 (2000).
- ³⁷P. J. Sarre, *Mon. Not. R. Astron. Soc.* **313**, L14–L16 (2000).
- ³⁸R. C. Fortenberry, *J. Phys. Chem. A* **119**, 9941–9953 (2015).
- ³⁹R. N. Compton, H. S. Carman, Jr., C. Desfrancois, H. Abdoul-Carime, J. P. Schermann, J. H. Hendricks, S. A. Lyapustina, and K. H. Bowen, *J. Chem. Phys.* **105**, 3472–3478 (1996).
- ⁴⁰F. Lecomte, S. Carles, C. Desfrancois, and M. A. Johnson, *J. Chem. Phys.* **113**, 10973–10977 (2000).
- ⁴¹T. Sommerfeld, *Phys. Chem. Chem. Phys.* **4**, 2511–2516 (2002).
- ⁴²L. Lehr, M. T. Zanni, C. Frischkorn, R. Weinkauff, and D. M. Neumark, *Science* **284**, 635–638 (1999).
- ⁴³J. P. Rogers, C. S. Anstöter, and J. R. R. Verlet, *Nat. Chem.* **10**, 341–346 (2018).
- ⁴⁴M. Gutowski, P. Skurski, X. Li, and L.-S. Wang, *Phys. Rev. Lett.* **85**, 3145–3148 (2000).
- ⁴⁵G. Liu, S. M. Ciburowski, C. R. Pitts, J. D. Graham, A. M. Buytendyk, T. Lectka, and K. H. Bowen, *Phys. Chem. Chem. Phys.* **21**, 18310 (2019).
- ⁴⁶G. Z. Zhu, Y. Liu, and L. S. Wang, *Phys. Rev. Lett.* **119**, 023002 (2017).
- ⁴⁷L.-S. Wang, *J. Chem. Phys.* **143**, 040901 (2015).
- ⁴⁸H.-T. Liu, C.-G. Ning, D.-L. Huang, and L.-S. Wang, *Angew. Chem., Int. Ed.* **53**, 2464–2468 (2014).
- ⁴⁹D.-L. Huang, H.-T. Liu, C.-G. Ning, and L.-S. Wang, *J. Chem. Phys.* **142**, 124309 (2015).
- ⁵⁰G.-Z. Zhu, C.-H. Qian, and L.-S. Wang, *J. Chem. Phys.* **149**, 164301 (2018).
- ⁵¹D.-L. Huang, H.-T. Liu, C.-G. Ning, G.-Z. Zhu, and L.-S. Wang, *Chem. Sci.* **6**, 3129–3138 (2015).
- ⁵²G.-Z. Zhu and L.-S. Wang, *Chem. Sci.* **10**, 9409–9423 (2019).
- ⁵³C.-H. Qian, G.-Z. Zhu, Y.-R. Zhang, and L.-S. Wang, *J. Chem. Phys.* **152**, 214307 (2020).
- ⁵⁴C.-H. Qian, Y.-R. Zhang, D.-F. Yuan, and L.-S. Wang, *J. Chem. Phys.* **154**, 094308 (2021).
- ⁵⁵R. S. Berry, *J. Chem. Phys.* **45**, 1228–1245 (1966).
- ⁵⁶J. Simons, *J. Am. Chem. Soc.* **103**, 3971–3976 (1981).
- ⁵⁷D.-L. Huang, H.-T. Liu, C.-G. Ning, and L.-S. Wang, *J. Phys. Chem. Lett.* **6**, 2153–2157 (2015).
- ⁵⁸G.-Z. Zhu, D.-L. Huang, and L.-S. Wang, *J. Chem. Phys.* **147**, 013910 (2017).
- ⁵⁹G. Z. Zhu, C. H. Qian, and L. S. Wang, *Angew. Chem., Int. Ed.* **58**, 7856–7860 (2019).
- ⁶⁰D. F. Yuan, Y. Liu, C. H. Qian, Y. R. Zhang, B. M. Rubenstein, and L. S. Wang, *Phys. Rev. Lett.* **125**, 073003 (2020).
- ⁶¹D.-F. Yuan, Y.-R. Zhang, C.-H. Qian, Y. Liu, and L.-S. Wang, *J. Phys. Chem. A* **125**, 2967–2976 (2021).
- ⁶²D.-F. Yuan, Y. Liu, C.-H. Qian, G. S. Kocheril, Y.-R. Zhang, B. M. Rubenstein, and L.-S. Wang, *J. Phys. Chem. Lett.* **11**, 7914–7919 (2020).
- ⁶³D. H. Kang, S. An, and S. K. Kim, *Phys. Rev. Lett.* **125**, 093001 (2020).
- ⁶⁴D. H. Kang, J. Kim, M. Cheng, and S. K. Kim, *J. Phys. Chem. Lett.* **12**, 1947–1954 (2021).
- ⁶⁵G.-Z. Zhu, L. F. Cheung, Y. Liu, C.-H. Qian, and L.-S. Wang, *J. Phys. Chem. Lett.* **10**, 4339–4344 (2019).
- ⁶⁶M. A. Yandell, S. B. King, and D. M. Neumark, *J. Chem. Phys.* **140**, 184317 (2014).
- ⁶⁷A. Kunin and D. M. Neumark, *Phys. Chem. Chem. Phys.* **21**, 7239–7255 (2019).
- ⁶⁸D. H. Kang, J. Kim, and S. K. Kim, *J. Phys. Chem. Lett.* **12**, 6383–6388 (2021).
- ⁶⁹L.-S. Wang, C.-F. Ding, X.-B. Wang, and S. E. Barlow, *Rev. Sci. Instrum.* **70**, 1957–1966 (1999).
- ⁷⁰X. B. Wang and L. S. Wang, *Rev. Sci. Instrum.* **79**, 073108 (2008).
- ⁷¹I. León, Z. Yang, H.-T. Liu, and L.-S. Wang, *Rev. Sci. Instrum.* **85**, 083106 (2014).
- ⁷²V. Dribinski, A. Ossadtchi, V. A. Mandelshtam, and H. Reisler, *Rev. Sci. Instrum.* **73**, 2634–2642 (2002).
- ⁷³G. A. Garcia, L. Nahon, and I. Powis, *Rev. Sci. Instrum.* **75**, 4989–4996 (2004).
- ⁷⁴M. J. Frisch, G. W. Trucks, H. B. Schlegel, G. E. Scuseria, M. A. Robb, J. R. Cheeseman, G. Scalmani, V. Barone, G. A. Petersson, H. Nakatsuji, X. Li, M. Caricato, A. Marenich, J. Bloino, B. G. Janesko, R. Gomperts, B. Mennucci, H. P. Hratchian, J. V. Ortiz, A. F. Izmaylov, J. L. Sonnenberg, D. Williams-Young,

F. Ding, F. Lipparini, F. Egidi, J. Goings, B. Peng, A. Petrone, T. Henderson, D. Ranasinghe, V. G. Zakrzewski, J. Gao, N. Rega, G. Zheng, W. Liang, M. Hada, M. Ehara, K. Toyota, R. Fukuda, J. Hasegawa, M. Ishida, T. Nakajima, Y. Honda, O. Kitao, H. Nakai, T. Vreven, K. Throssell, J. A. Montgomery, Jr., J. E. Peralta, F. Ogliaro, M. Bearpark, J. J. Heyd, E. Brothers, K. N. Kudin, V. N. Staroverov, T. Keith, R. Kobayashi, J. Normand, K. Raghavachari, A. Rendell, J. C. Burant, S. S. Iyengar, J. Tomasi, M. Cossi, J. M. Millam, M. Klene, C. Adamo, R. Cammi, J. W. Ochterski, R. L. Martin, K. Morokuma, O. Farkas, J. B. Foresman, and D. J. Fox, Gaussian 09, Revision D.01, Gaussian, Inc., Wallingford, CT, 2016.

⁷⁵I. Pugliesi and K. Müller-Dethlefs, *J. Phys. Chem. A* **110**, 4657–4667 (2006).

⁷⁶S. T. Edwards, M. A. Johnson, and J. C. Tully, *J. Chem. Phys.* **136**, 154305 (2012).

⁷⁷J. Czekner, L. F. Cheung, G. S. Kocheril, and L.-S. Wang, *Chem. Sci.* **10**, 1386–1391 (2019).

⁷⁸D.-L. Huang, H.-T. Liu, C.-G. Ning, P. D. Dau, and L.-S. Wang, *Chem. Phys.* **482**, 374–383 (2017).

⁷⁹D. J. Nesbitt and R. W. Field, *J. Phys. Chem.* **100**, 12735–12756 (1996).

⁸⁰Y. Yamada, J.-i. Okano, N. Mikami, and T. Ebata, *J. Chem. Phys.* **123**, 124316 (2005).

⁸¹J. A. Frey, R. Leist, C. Tanner, H.-M. Frey, and S. Leutwyler, *J. Chem. Phys.* **125**, 114308 (2006).

⁸²S. Karmakar and S. Keshavamurthy, *Phys. Chem. Chem. Phys.* **22**, 11139 (2020).